© 2018. This manuscript version is made available under the CC-BY-NC-ND 4.0 license
http://creativecommons.org/licenses/by-nc-nd/4.0/

Unmodified and multi-walled carbon nanotube modified tetrahedral amorphous carbon (ta-C) films as in vivo sensor materials for sensitive and selective detection of dopamine

Tommi Palomäki[a], Emilia Peltola[a], Sami Sainio[b], Niklas Wester[b], Olli Pitkänen[c], Krisztian Kordas[c], Jari Koskinen[b], Tomi Laurila[a*]

[a]Department of Electrical Engineering and Automation, School of Electrical Engineering, Aalto University, P.O. Box 13500, 00076 Aalto, Finland

[b]Department of Chemistry and Materials Science, School of Chemical Technology, Aalto University, P.O. Box 16100, 00076 Aalto, Finland

[c]Microelectronics Research Unit, Faculty of Information Technology and Electrical Engineering, University of Oulu, P.O. Box 8000, FI-90014 Oulu, Finland

*Corresponding author: Tomi Laurila
E-mail: tomi.laurila@aalto.fi
Telephone: +358 503414375
Address: Department of Electrical Engineering and Automation, School of Electrical Engineering, Aalto University, P.O. Box 13500, 00076 Aalto, Finland

Abstract

Unmodified and multi-walled carbon nanotube (MWCNT) modified tetrahedral amorphous carbon (ta-C) films of 15 and 50 nm were investigated as potential in vivo sensor materials for the detection of dopamine (DA) in the presence of the main interferents, ascorbic acid (AA) and uric acid (UA). The MWCNTs were grown directly on ta-C by chemical vapor deposition (designated as ta-C+CNT) and were characterized with X-ray photoelectron spectroscopy, Raman spectroscopy, scanning and transmission electron microscopy. Electroanalytical sensitivity and selectivity were determined with cyclic voltammetry. Biocompatibility of the materials was assessed with cell cultures of mouse neural stem cells (mNSCs). The detection limits of DA for both ta-C and ta-C+CNT electrodes ranged from 40 to 85 nM, which are well within the required range for in vivo detection. The detection limits were lower for both ta-C and ta-C+CNT electrodes with 50 nm of ta-C compared to 15 nm. The ta-C electrodes showed a large dynamic linear range of 0.01-100 µM but could not resolve between the oxidation peaks of DA, AA and UA. Modification with MWCNTs, however, resulted in excellent selectivity and all three analytes could be detected simultaneously at physiologically relevant concentrations using cyclic voltammetry. Based on cell culture of mNSCs, both ta-C and ta-C+CNT exhibited good biocompatibility, demonstrating their potential as in vivo sensor materials for the detection of DA.

Keywords: tetrahedral amorphous carbon, multi-walled carbon nanotubes, dopamine, ascorbic acid, cyclic voltammetry, biocompatibility

1. Introduction

Tetrahedral amorphous carbon (ta-C), a form of highly sp^3-bonded diamond-like carbon, has increasingly found use in electroanalytical applications due to its favorable electrochemical properties resembling those of diamond. These include a wide potential window, low background current and chemical inertness. (Laurila et al., 2014, Zeng et al., 2014, X. Yang et al., 2012, Yoo et al., 1999) The significant advantage compared to diamond is the low deposition temperature that allows the use of a variety of substrate

materials and the compatibility with semiconductor fabrication processes (Yoo et al., 1999). ta-C is also an attractive material for use in vivo, because of its good biocompatibility (Kaivosoja et al., 2013), resistivity to bacterial adhesion (Levon et al., 2010) and fouling (Goto et al., 2011), and good mechanical properties (Robertson, 2002). ta-C has been used to measure biomolecules such as dopamine (Palomäki et al., 2015, Laurila et al., 2014, Medeiros et al., 2013, Sopchak et al., 2002), norepinephrine (Qiu et al., 2015), glucose (G. Yang et al., 2009, Maalouf et al., 2006), tryptophan, tyrosine (Jarošová et al., 2016), HIV and hepatitis (Kim et al., 2009), as well as heavy metals (Khun and Liu, 2009, Liu and Liu, 2005). In most cases, ta-C has been doped with nitrogen, nickel or boron to improve the electrical properties but we have recently shown that undoped ta-C can also achieve high charge transfer rates by adjusting the thickness of the ta-C film and using a Ti adhesion layer (Palomäki et al., 2017).

Dopamine (DA) is an important neurotransmitter that conveys cognitive, behavioral and motor functions and it is involved in several neurological disorders such as Parkinson's disease, schizophrenia, Tourette's syndrome and addiction (Tritsch and Sabatini, 2012). The detection of DA in physiological conditions is challenging due to its very low concentrations in the nanomolar range compared to the main interferents, ascorbic acid (AA) and uric acid (UA), typically present at orders of magnitude higher concentrations. While several carbon-based electrodes can achieve the required sensitivity, the lack of selectivity remains the main challenge to overcome. Modification of conventional electrodes such as gold, platinum or glassy carbon (GC) with metal nanoparticles (Tsierkezos et al., 2016, Dursun and Gelmez, 2010), nanodiamonds (Peltola, Wester et al., 2017, Holt et al., 2008), carbon nanotubes (Tan et al., 2018, Sainio et al., 2015), carbon nanofibers (Huang et al., 2008) and graphene (Wester et al., 2017, Sun et al., 2011) generally improves selectivity even though the underlying reasons are still not well understood (Pumera, 2012, Dumitrescu et al., 2009). In addition, the modification of conventional electrodes by carbon nanomaterials is usually done by dropcasting, which allows for very limited control over the overall structure of the modified electrode and thus its physical properties (Tan et al., 2018, Laurila et al., 2017). This complicates the understanding of the relationship between material properties and their electroanalytical performance, and more importantly adds concerns about the possible release and toxicity of nanoparticles bonded with weak van der Waals forces on the substrate.

In this study, we have investigated the use of 15 and 50 nm thick undoped ta-C films as potential in vivo sensor materials for the detection of dopamine in the presence of AA and UA at physiological concentrations. Both ta-C films were modified by growing multi-walled carbon nanotubes (MWCNTs) to compare their electroanalytical performance and biocompatibility. In order to obtain more control over the electrode structure and improve repeatability of the fabrication process, the MWCNTs were grown by chemical vapor deposition (CVD) directly on top of ta-C. The direct growth of MWCNTs on the surface of ta-C not only helps ensure high repeatability of the fabrication process but also guarantees sufficient electrical interface between the carbon nanomaterials and grants proper mechanical integrity without serious concerns about the release of carbon nanotubes in vivo. The 15 and 50 nm films were chosen based on their different electrochemical properties: the 15 nm ta-C film has a lower sp^2/sp^3 fraction that leads to faster electron transport through the film compared to the 50 nm film (Palomäki et al., 2017). In addition, from a previous TEM investigation of the ta-C/MWCNT interface (Laurila et al., 2015), it was observed that the 15 nm film was consumed during the CVD growth process. Therefore, the 50 nm film was chosen for comparison to see to what extent it would stay intact (if at all) and what would be its possible implication in the physical and electrochemical properties of the modified electrode. X-ray photoelectron spectroscopy (XPS), Raman spectroscopy, scanning and transmission electron microscopy (SEM and TEM) were used to characterize the electrodes and their electroanalytical performance was tested using cyclic voltammetry. Furthermore, mouse neural stem cells (mNSCs) were cultured on ta-C and ta-C+CNT films to assess their biocompatibility for use as in vivo sensors.

2. Materials and methods

2.1. Deposition of ta-C

A 20 nm Ti adhesion layer was deposited by direct-current magnetron sputtering on highly conductive (0.001-0.002 Ω cm) p-type (100) Si wafers (Ultrasil). ta-C thin films of 15 and 50 nm were deposited on top of the Ti adhesion layer by filtered cathodic vacuum arc in the same deposition chamber. Further details can be found in the supplementary information.

2.2. Deposition of MWCNTs

A multilayer catalysts film of 0.2 nm Al, 3 nm Co and 3 nm Fe was deposited on the top of ta-C by RF-sputtering and e-beam evaporation. The samples were then placed in a low pressure chemical vapor deposition (CVD) reactor (Aixtron, Black Magic) and heated to 550 °C process temperature using an electrical heated graphite holder in NH_3 (250 sccm) at 10 mbar pressure for 10 min to reduce catalyst metals. The reactor chamber was then evacuated and subsequently filled with N_2 buffer gas (250 sccm) back to 10 mbar process pressure. Next, the carbon precursor (C_2H_2) was introduced into the chamber (25 sccm) for another 10 min for the MWCNT synthesis while keeping the temperature at 550 °C. The obtained samples were labeled either 15 nm ta-C+CNT or 50 nm ta-C+CNT depending on the ta-C film thickness.

2.3. Characterization methods

The morphology of the ta-C+CNT samples was examined by scanning electron microscopy (Hitachi S-4700). The microstructure of the cross-sectional samples was investigated with a transmission electron microscope (JEOL JEM-2200FS) equipped with an energy-dispersive X-ray spectroscope (EDS) for elemental analysis. Cross-sectional samples were prepared by focused ion beam (FIB).

X-ray photoelectron spectroscopy (AXIS Ultra, Kratos Analytical) was used for analyzing the surface chemical composition of the samples. Elemental carbon to oxygen ratios in the surface region were determined from wide spectra collected using 1 eV step and 80 eV pass energy. High-resolution C 1s spectra were collected using 0.1 eV step and 20 eV pass energy. All spectra were collected using monochromatic Al Kα x-ray source at 100 W and with neutralization in the case of charging. Samples were pre-evacuated overnight in vacuum $<10^{-5}$ Pa. Analysis chamber vacuum was $<10^{-6}$ Pa during measurements. Spectra for each sample were collected from at least three locations (analysis area ~400 x 800 µm, depth <10 nm). Filter paper (100% cellulose, Whatman) was used as in situ reference and for binding energy scale calibration (CO = 286.7 eV, C-C = 285.0) (Johansson and Campbell, 2004, Beamson and Briggs, 1992). Data fitting, atomic composition ratio calculations and charge correction was done using CasaXPS software (v. 2.3.18).

Visible Raman spectra were acquired with a LabRAM HR (Jobin Yvon Horiba) equipped with a BX41 microscope (Olympus) and a 100x objective at an excitation wavelength of 514 nm and 10 mW power.

2.4. Electrochemical measurements

Cyclic voltammetry was carried out with a Gamry Reference 600 potentiostat in a three-electrode setup with an Ag/AgCl reference electrode (+0.199 V vs SHE, Radiometer Analytical) and a Pt wire as counter electrode. All the solutions were prepared on the day of the measurement, purged with Argon for at least 15 min and blanketed during experiments. New electrodes were used for each measurement. L-ascorbic acid, uric acid and dopamine hydrochloride were purchased from Sigma-Aldrich and dissolved in phosphate buffer solution (PBS) with pH 7.4. All measurements were done at room temperature. The geometric area of the electrodes was 0.071 cm^2.

2.5. Evaluation of biocompatibility

The samples were sterilized in 70% ethanol for 10 min prior to cell culture experiments. Cells were cultured in humidified incubator with 5% CO_2 in the air. Mouse neural stem cells (mNSC, ATCC® CRL2926™) were cultured in Eagle's Minimum Essential Medium (without phenol red) supplemented with 4 mM L-Glutamine, 10 % FBS, 100 IU/ml of penicillin and 100 µg/ml of streptomycin. The seeding density was 34 000 cells cm^{-2}, which is the recommended seeding density for mNSCs. The cells were cultured on the samples placed in 12-well plates for 24 hours.

Acting cytoskeleton was stained after 4% paraformaldehyde fixation and 0.5% triton-X permeabilization using phalloidin-568-label (Biotium 1:50 in PBS, 30 min incubation) and nuclei by DAPI (Vectrashield mounting medium with DAPI). Olympus BX51M microscope and Leica DCF420 digital microscope camera were used for the cell morphology imaging. Cell count was calculated from nuclei staining of four images per sample type.

3. Results and discussion

3.1. SEM

The SEM images (Fig. 1 A and B) showed that a mostly uniform mesh of intertwined and several micrometers long MWCNTs had grown on both 15 and 50 nm ta-C films after the CVD process. The diameter of the MWCNTs was 20-40 nm. The MWCNT mesh appeared denser and the diameter of the MWCNTs slightly smaller on the 50 nm ta-C film. Small variations in the thickness and density of MWCNTs are expected in the CVD process due to the unevenness of the ta-C and catalyst layers.

3.2. TEM

Several differences in the cross-sectional TEM images (Fig. 1 C and D) were observed between the MWCNTs deposited on 15 and 50 nm ta-C films. In the 15 nm ta-C+CNT sample, the Ti interlayer was intact and had a thickness of around 25 nm. The MWCNTs seemed to have grown from the Ti interlayer consuming the ta-C layer since it was no longer observed after the CVD process. In the 50 nm ta-C+CNT sample, on the other hand, a 50-60 nm thick disordered graphite-like carbon layer was seen on top of Ti. The Ti interlayer was continuous but was thinner (around 15 nm) than in the 15 nm ta-C+CNT sample. The carbon layer contained numerous metal nanoparticles that were confirmed with EDS to be a mixture of Fe and Co catalysts, as well as MWCNT-type structures embedded in the layer. Several dark regions at the interface between Ti and Si were identified as Fe silicides with dissolved Co (indicated as (FeCo)Si in Fig. 1 D). All in all, the interfacial region in the 50 nm ta-C+CNT sample contained significantly more metal nanoparticles than the 15 nm ta-C+CNT sample. However, in both samples, metal nanoparticles were observed also at the end of the MWCNTs. A more detailed analysis of the interfacial region can be found in our previous report (Laurila et al., 2015).

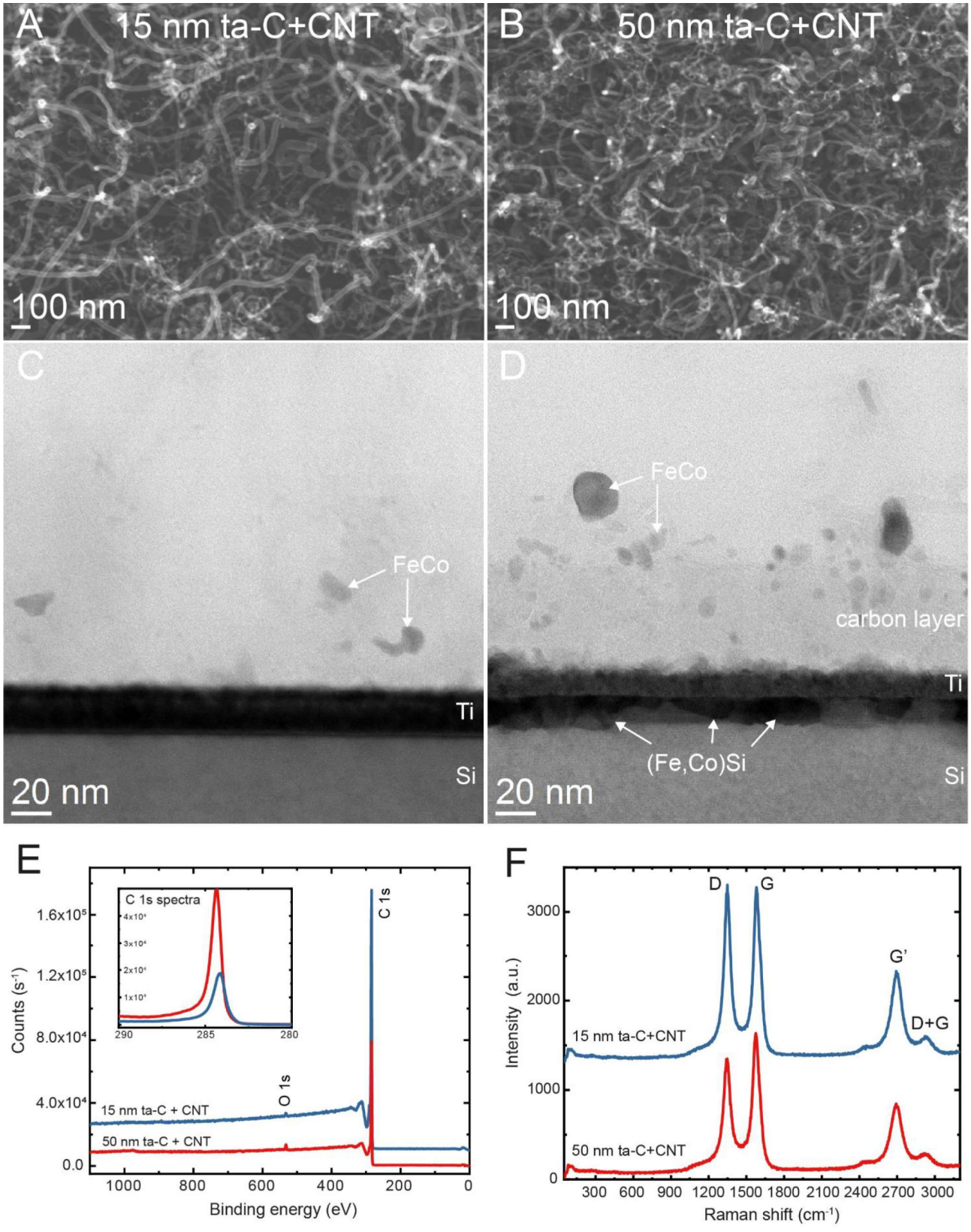

Figure 1. *A, B) SEM images. C, D) cross-sectional TEM micrographs. A and C represent the 15 nm ta-C+CNT sample while B and D the 50 nm ta-C+CNT sample. E) XPS wide spectra (with C 1s spectra as insets) and F) Raman spectra of the ta-C+CNT samples.*

3.3. XPS

Surface elemental analysis determined from XPS wide spectra (Fig. 1E) indicated that the ta-C+CNT samples were composed of graphitic carbon and a very small amount of oxygen (99.6 at.% and 0.4 at.% for 15 nm ta-C+CNT, and 98.5 at.% and 1.6 at.% for 50 nm ta-C+CNT, respectively). The metal catalysts (Al, Fe, Co) used in the growth of MWCNTs could not be detected within the depth of analysis (about 10 nm) in either sample. However, based on TEM micrographs, we know that metal nanoparticles are present in the interfacial region between Si and MWCNTs and at the tube ends. It is possible that the amount of metal nanoparticles inside the MWCNTs and in the mesh structure is below the limit of detection. The mesh is also much thicker than the depth of analysis and therefore XPS does not give any information from the interfacial area. It also explains why Ti was not observed in the XPS wide spectra.

3.4. Raman spectroscopy

The Raman spectra (Fig. 1 F) showed the characteristic features of MWCNTs with a G band (1575 cm^{-1}) and a D band (1345 cm^{-1}) in the first-order spectra and a G' band (2695 cm^{-1}) and D+G combination mode (2920 cm^{-1}) in the second-order spectra. (Bokobza et al., 2013, Antunes et al., 2006) The G band arises from sp^2-bonded carbon atoms in rings and olefinic chains whereas the D and D+G bands are induced by disorder. The G' band is an overtone of the D band and it is not related to disorder. (Pimenta et al., 2007) The ratio of intensities of the D and G bands is widely used for characterizing the quantity of defects in graphitic materials and can be used to estimate the degree of structural integrity of the MWCNTs (Antunes et al., 2006). The relatively high I_D/I_G ratios of around 1.0 and 0.80 for 15 nm ta-C+CNT and 50 nm ta-C+CNT, respectively, indicated a high defect density which is expected at the low growth temperature of 550 °C. The clear difference in I_D/I_G also indicated that the 15 nm ta-C+CNT sample is more defective.

3.5. Sensitivity

Cyclic voltammetry (CV) has been used extensively for the detection of dopamine in vivo because it can achieve a high temporal resolution despite lower sensitivity and selectivity compared to other techniques such as differential pulse voltammetry (DPV) and square-wave voltammetry (SWV). (Robinson et al., 2008) High temporal resolution is necessary for the measurement of fast dopamine transients that occur in neuronal synapses (Mark Wightman, 1988). Therefore, CV was used instead of DPV or SWV for sensitivity and selectivity measurements to obtain results that are more relevant for in vivo sensor applications.

The CVs presenting the sensitivity of the ta-C and ta-C+CNT electrodes towards DA are shown in Fig. 2. Both ta-C and ta-C+CNT electrodes could detect nanomolar levels of dopamine corresponding to physiologically relevant concentrations. The concentration of DA in the extracellular fluid of the brain varies from basal concentrations of 5-60 nM (Justice Jr, 1993, Ross, 1991, Mark Wightman, 1988) to transients of 200-500 nM following natural stimuli (Robinson et al., 2002, Robinson, 2001) or up to 1 mM following evoked stimuli using implanted electrodes (Ford et al., 2010).

The 15 nm ta-C electrode had a sensitivity of 0.28 A M^{-1} cm^{-2} with a relative standard deviation (RSD) of 1.17 and the 50 nm ta-C electrode 0.52 A M^{-1} cm^{-2} with an RSD of 0.45. The sensitivity of unmodified ta-C electrodes was higher than that of the 15 nm ta-C+CNT electrode with 0.08 A M^{-1} cm^{-2} and an RSD of 0.93, and the 50 nm ta-C+CNT electrode with 0.07 A M^{-1} cm^{-2} and an RSD of 0.19. The linear range was 0.01-100 µM for both ta-C electrodes, 0.01-5 µM for the 15 nm ta-C+CNT and 0.05-10 µM for the 50 nm ta-C+CNT. The sensitivity and linear range values are shown in Table 1 and the calibration curves are shown in the insets of Fig. 2. The observed differences in sensitivity between unmodified and modified electrodes may be explained by the drastically different surface morphology and chemistry of the materials that strongly affect the adsorption behavior of DA, which is a known inner-sphere redox probe (McCreery, 2008).

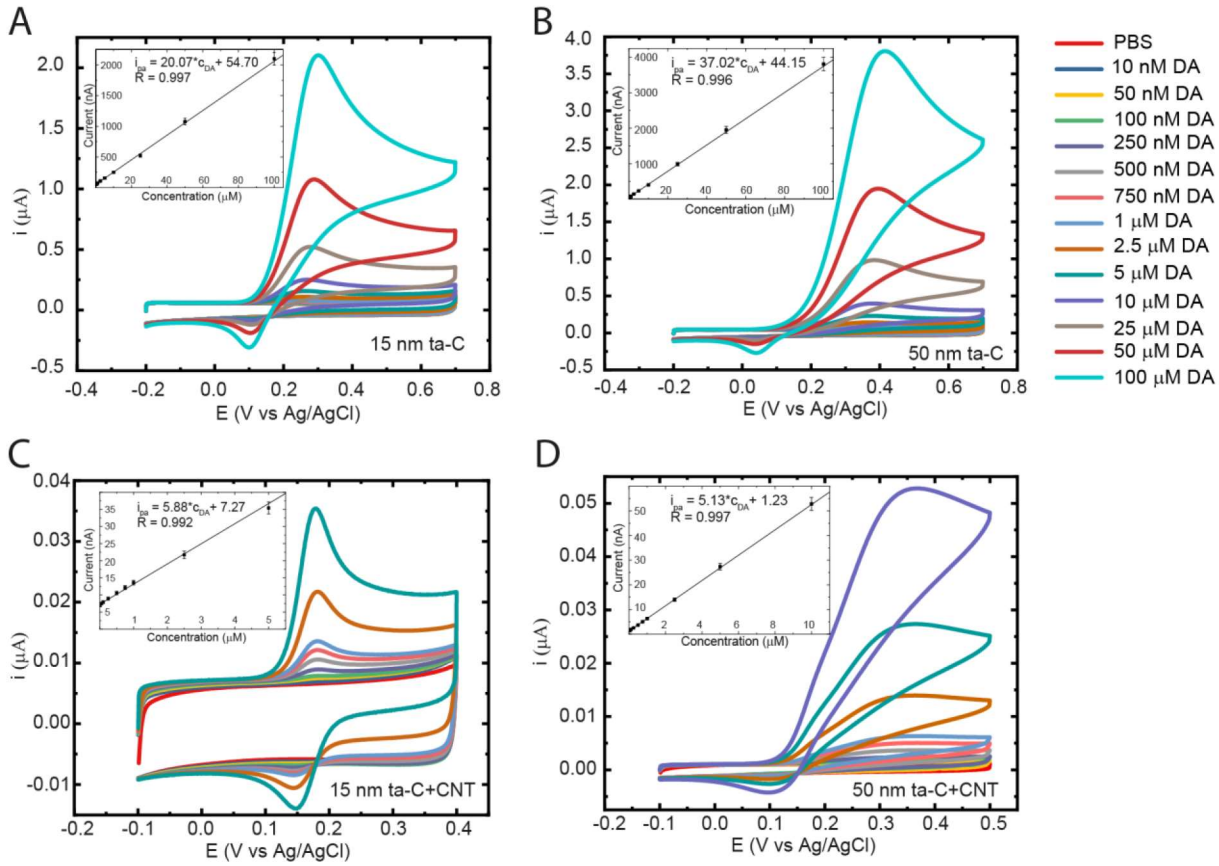

***Figure 2**. Cyclic voltammograms showing the sensitivity of A) 15 nm ta-C, B) 50 nm ta-C, C) 15 nm ta-C+CNT and D) 50 nm ta-C+CNT electrodes. Insets show the calibration curves (refer to Table 1 for linear range values). Scan rate 50 mV/s.*

The limit of detection (LOD) was calculated using the equation: LOD = 3.3 × σ/S (where σ is the standard deviation of the blank CVs and S the sensitivity). The results are tabulated in Table 1. The LOD values for the 15 nm ta-C and 50 nm ta-C electrodes were 84.3 ± 14 and 39.8 ± 5.9 nM, respectively. Interestingly, the modification of ta-C with MWCNTs did not improve the limit of detection, resulting in 76.7 ± 4.6 nM for 15 nm ta-C+CNT and 41.4 ± 0.4 nM for 50 nm ta-C+CNT. The ta-C and ta-C+CNT electrodes with 50 nm of ta-C had better LOD values resulting from a lower capacitive background current as well as a smaller standard deviation of the blank CVs compared to the corresponding electrodes with 15 nm of ta-C. In the case of the 50 nm ta-C electrode, this is due to the higher fraction of sp^3-bonded carbon when the ta-C film is thicker, leading to electrochemical properties closer to diamond-like carbon (Palomäki et al., 2017). In the case of the 50 nm ta-C+CNT electrode, the additional disordered graphite-like carbon layer seen in TEM micrographs (Fig. 1 D) could play a similar role in lowering the capacitive background current but this needs to be investigated further in future work. It is to be noted that the higher sensitivity of the unmodified ta-C electrodes was offset by the larger standard deviation of their blank CVs, thus roughly equalizing the LOD values between the 15 nm ta-C and ta-C+CNT electrodes and between the 50 nm ta-C and ta-C+CNT electrodes. The calculated LOD values corresponded well to the lowest experimentally observed current responses to dopamine (50-100 nM). Finally, it should be noted that the variation in the (unknown) electrochemically active area of the electrodes will affect the calculated sensitivity and LOD values of the modified electrodes at least to some degree.

Table 1. *Electrochemical data. The oxidation potentials of DA, AA and UA were measured for each analyte separately in PBS at 50 mV/s (Fig 3 A and B show the CVs for 15 nm ta-C and 15 nm ta-C+CNT). Linear range, sensitivity and LOD values were calculated from the CVs in Fig. 2.*

Electrode	E_{pa} (V)			Linear range (µM)	Sensitivity (A M^{-1} cm^{-2})	LOD (nM)
	100 µM DA	1 mM AA	50 µM UA			
15 nm ta-C	0.32	0.56	0.59	0.01-100	0.28	84.3 ± 14
50 nm ta-C	0.38	0.67	0.64	0.01-100	0.52	39.8 ± 5.9
15 nm ta-C+CNT	0.19	0.00	0.34	0.01-5	0.08	76.7 ± 4.6
50 nm ta-C+CNT	0.17	0.00	0.37	0.05-10	0.07	41.4 ± 0.4

Comparing the limit of detection of the ta-C electrodes to similar unmodified materials in literature (Table 2), we found that the obtained LODs were better than at boron-doped diamond (BDD), nitrogen-doped amorphous carbon (a-C:N) and nitrogen-doped tetrahedral amorphous carbon (ta-C:N). The LOD values of the ta-C+CNT electrodes were compared to various modified electrodes that can simultaneously detect DA in the presence of AA and UA using CV (Table 2). The comparison was limited to electrodes that use carbon nanomaterials and achieve selectivity using CV. The comparison shows that the obtained LOD values are among the best found in literature. It should also be noted that the values for several electrodes have been obtained with more sensitive voltammetric methods such as DPV, SWV or amperometry. This further underlines the excellent LOD values of both ta-C and ta-C+CNT electrodes obtained with CV and shows their applicability for in vivo detection of DA.

3.6. Selectivity

Selectivity of the ta-C and ta-C+CNT electrodes was tested in a ternary solution containing 1 mM ascorbic acid, 50 µM uric acid and varying amounts of dopamine. These concentrations correspond approximately to the maximum physiological concentrations of AA and UA found in the human brain (Rice, 2000, Reiber et al., 1993).

The ta-C electrodes could not differentiate between the three analytes as can be seen in Fig. 3 A for 15 nm ta-C (and in Fig. S1 for 50 nm ta-C). In the ternary solution, only one peak appeared for the oxidation of AA, UA and DA. Looking at the CVs of the individual analytes, the oxidation peaks of AA and UA completely overlap whereas the oxidation peak of DA cannot be resolved because its magnitude is much smaller than that of AA at physiologically relevant concentrations. The oxidation potentials (E_{pa}) of each analyte are given in Table 1. The lack of selectivity is a long-standing problem that has been observed at many conventional electrodes such as carbon paste (Huang et al., 2008), GC (Zhang et al., 2017) and Pt (Tsierkezos et al., 2016, Wang et al., 2011).

It is to be noted that the current of the single oxidation peak in ternary solution is larger than that of the individual peaks combined. This is explained at least in part by the regeneration of uric acid (Kohen and Nyska, 2002) and dopamine (Robinson et al., 2008) by AA that acts as a strong antioxidant. Uric acid diimine and dopamine quinone (the oxidized forms of UA and DA respectively) are reduced back to their original forms before they undergo further chemical reactions and can thus re-oxidize at the electrode surface.

Compared to the unmodified ta-C electrodes, the ta-C+CNT electrodes showed three clearly defined oxidation peaks in the ternary solution (Fig. 3 C and D), corresponding to those of each analyte measured separately (Fig. 3 B). Here, in addition to the regeneration of DA and UA, their responses are superimposed on the diffusion tail of AA, increasing their total current. This can be seen clearly in Fig. 3 C and D, where

the concentration of DA has been increased stepwise from 1 to 100 µM. The excellent selectivity observed at the ta-C+CNT electrodes is due to the large negative shift in the oxidation potential of AA (from 0.58 V at ta-C to 0.0 V vs Ag/AgCl at ta-C+CNT). The oxidation potentials of UA and DA also shift negatively but much less than that of AA, enabling large enough a peak potential separation between each analyte for their simultaneous determination (Table 1).

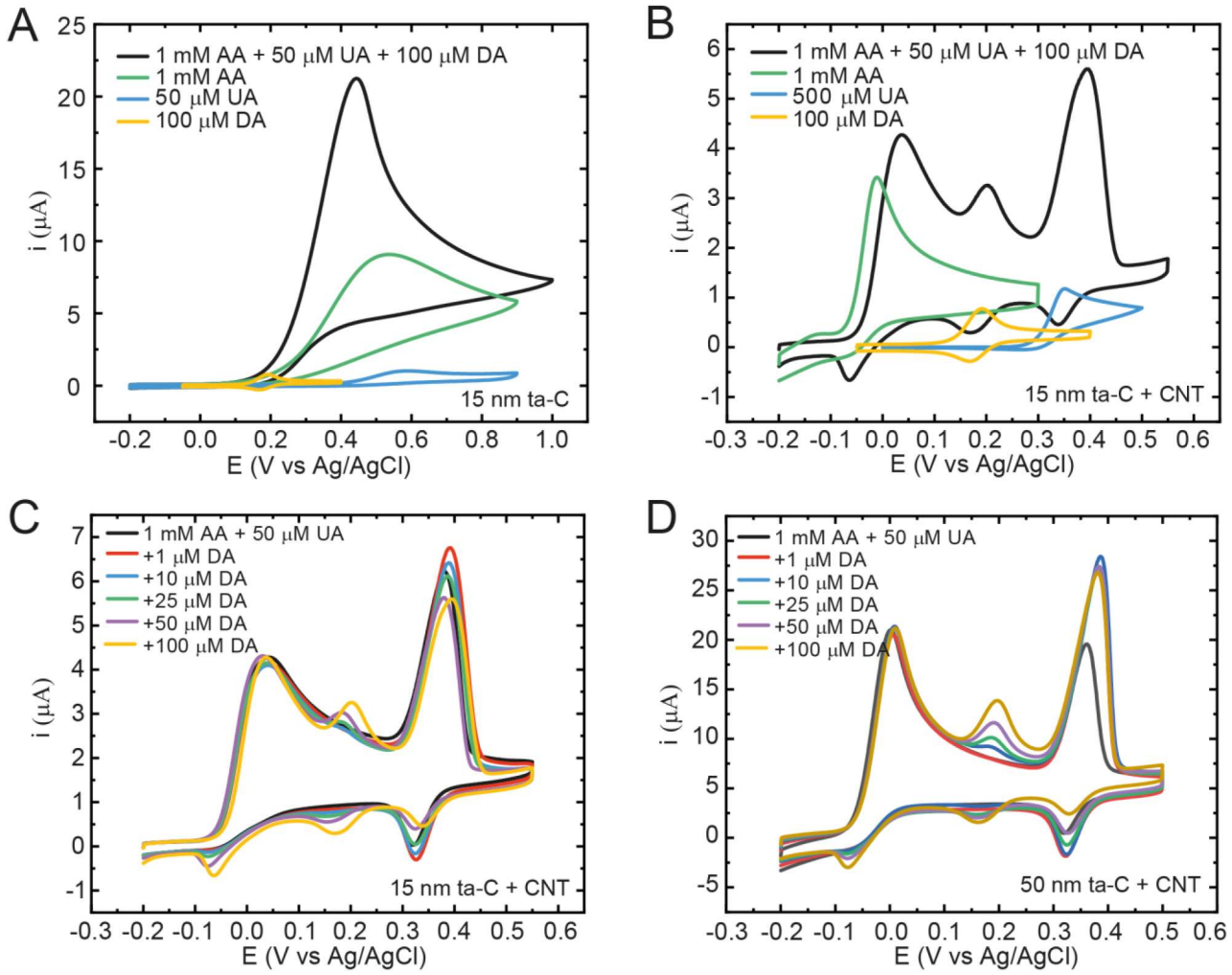

***Figure 3**. Cyclic voltammograms showing the selectivity of the A) 15 nm ta-C and B) 15 nm ta-C+CNT electrodes in a ternary solution composed of 1 mM AA, 50 µM UA and 100 µM DA in PBS (black curve). In the same images, the CVs of each analyte measured separately at the same concentrations (except 500 µM UA at the ta-C+CNT electrode) are superimposed. The concentration of dopamine was increased from 1 to 100 µM in the presence of 1 mM AA and 50 µM UA at the C) 15 nm ta-C+CNT and D) 50 nm ta-C+CNT electrodes. Scan rate 50 mV/s.*

At all the modified electrodes listed in Table 2, DA can be selectively determined in the presence of AA and UA using cyclic voltammetry. In each case, the selectivity is achieved by shifting the oxidation potential of AA in the cathodic direction. The shift is generally attributed to the catalytic effect of the modifying carbon nanomaterials due to their electronic properties and large amount of edge-plane or defective sites. However, it has been suspected that the metal nanoparticles (NPs) used as catalysts in the growth of carbon nanomaterials and nanographite impurities are actually the cause of the catalytic effect. (Ma et al., 2014, Pumera, 2012, Scott and Pumera, 2011, Dumitrescu et al., 2009) In fact, Tsierkezos et al. (2016)

showed that N-doped MWCNTs can selectively detected DA in the presence of AA and UA with a LOD of 1.4 µM. The selectivity and LOD could be further enhanced by modifying the electrode with Rh, Pd, Ir, Pt or Au NPs. Modification with Au NPs resulted in the lowest LOD (0.3 µM) and largest negative shift of the oxidation potential of AA. (Tsierkezos et al., 2016)

Shang et al. (2008) demonstrated selective determination of AA, DA and UA at multilayer graphene nanoflake films (MGNFs) whose electrocatalytic activity was attributed to the abundance of edge planes, defects and negatively charged oxygen functional groups. Since the MGNFs were free of metal catalysts, their contribution could be ruled out. The surface termination with appropriate functional groups can repel the anionic AA and UA molecules and attract the cationic DA molecule due to electrostatic effects to confer selectivity to the electrode. For example, Oh et al. (2016) showed that modification of GC/MWCNT surface with citric acid introduced negatively charged carboxylate groups that suppressed almost entirely the signal of ascorbic acid and enhanced that of dopamine compared to bare GC/MWCNT. Surface modification with protonated amine groups had the opposite effect. (Oh et al., 2016)

Table 2. *Non-exhaustive list of publications where AA, DA and UA have been simultaneously detected using CV. LOD values calculated with CV are reported if they were given in the original reports.*

Electrode	LOD (nM)	Linear range (µM)	Method	Ref
Unmodified electrodes				
ta-C	1000[a]	-	CV	(Laurila et al., 2014)
ta-C:N	100-200	-	HMRDE	(Sopchak et al., 2002)
a-C:N	65.6	0.08-8.3	SWV	(Medeiros et al., 2013)
BDD	283	0.49-5.4	SWV	
BDD	147	-	FSCV	(Yoshimi et al., 2011)
Nb/N-DLC	500[a]	0.5-20	DPV	(Liu et al., 2017)
15 nm ta-C	39.4	0.01-100	CV	this work
50 nm ta-C	31.4	0.01-100	CV	this work
Modified electrodes				
N-MWCNT/Au NPs	300	12-322	CV	(Tsierkezos et al., 2016)
Pt/CNS	120	0.8-2 and 2-100	CV	(Wang et al., 2011)
Si/MGNFs	170	1-50 and 50-100	DPV	(Shang et al., 2008)
GCE/MWCNT/Pt NPs	27.8	0.043-62	DPV	(Dursun and Gelmez, 2010)
GCE/MWCNT/PDOP/Pt NPs	8800	30-120	CV	(M. Lin et al., 2013)
	80	0.25-20	DPV	
OMC/Nafion/GCE	500	1-90	DPV	(Zheng et al., 2009)
Graphene/Pt NPs/GCE	30	0.03-8.13	Amp	(Sun et al., 2011)
poly-Evans Blue/GCE	300	1-30	DPV	(L. Lin et al., 2008)
UIO-66/CB/GCE	5	0.03-2	DPV	(W. Zhang et al., 2017)
rGO/CNT/ITO	40	0.2-8	DPV	(Y. Zhang et al., 2015)
15 nm ta-C +CNT	30.6	0.01-5	CV	this work
50 nm ta-C + CNT	35.9	0.05-10	CV	this work

[a] lowest detected response experimentally (not a calculated LOD value)
Electrode explanations: carbon nanosheets (CNS), multilayer graphene nanoflake films (MGNFs), polydopamine (PDOP), ordered mesoporous carbon (OMC), UIO-66 metal organic framework, carbon black (CB), reduced graphene oxide (rGO), indium tin oxide (ITO)

Henstridge et al. (2010) reported that a change in diffusion regime from planar to thin film diffusion inside a porous layer of conducting material can also account for a cathodic shift in oxidation potential. They demonstrated this by using computational simulations and experimentally by measuring dopamine at MWCNT-modified glassy carbon electrodes. A thicker MWCNT film reduced the peak-to-peak separation by lowering the overpotential for both oxidation and reduction. Therefore, instead of an electrocatalytic effect tied to a change in electrode kinetics, a change in diffusion regime may also cause an improvement in selectivity. However, thin layer diffusion cannot be distinguished from adsorption that also causes lowering of the peak-to-peak separation.

In the case of our ta-C+CNT electrodes, we cannot say unambiguously what causes the oxidation potential of AA to shift negatively, because the MWCNTs contain edge-plane sites, defects, metal NPs and they form a mesh that acts as a porous conductive layer that may lead to thin layer diffusion as described above. Recent results have shown that modifying ta-C with Fe particles lowers the oxidation potential of AA but the cause cannot be attributed solely to Fe, because there is an accompanying change in bonding structure from sp^3 to sp^2 in ta-C. Therefore, the electrical and electronic properties in the bulk of the ta-C film also change resulting in enhanced electron transport through the layer (Etula et al., 2018).

Interestingly, we have observed that the oxidation potential of AA is not automatically shifted at new ta-C+CNT electrodes. The electrodes need to be pretreated either by cycling to around 0.8-1.0 V (vs Ag/AgCl) (Fig. S2 B and C) or by HNO_3-pretreatment (Fig. S2 A). The progressive increase of the upper potential limit of CV in 1 mM AA (Fig. S2 C) can be seen to cause a large oxidation peak to appear around 0.8-0.9 V. As the potential is further increased, the oxidation peak of AA slowly starts to shift in the negative direction (or another peak gradually appearing around 0.0 V is merged with the original one). This would indicate that a modification of surface chemistry or a structural change induced by either pretreatment is necessary to lower the overpotential of AA to confer selectivity. It has been shown that HNO_3-pretreatment causes defects and increases oxygen functional groups on the surface of CNTs which affect in particular the oxidation of AA (Gusmão et al., 2016). Also, Pumera et al. (2008) showed that electrochemical oxidation of CNTs resulted in more edge-plane defects and an increase in oxygen functional groups, in particular carboxyl groups. Therefore, it is possible that an increase in certain types of oxygen functional groups and defects could contribute to the shift in AA oxidation potential also in our case. Cycling in PBS also induces the same effect and it is accompanied by a new pair of redox peaks at 0.05 V (Fig. S2 B). This could also be related to the oxidation and reduction of metal nanoparticles. In any case, the slow shift in AA oxidation potential observed in Fig. S2 C would exclude the hypothesis of a change in diffusion regime brought by the mesh of MWCNTs.

3.7. Evaluation of biocompatibility

Tetrahedral amorphous carbon thin films are known to exhibit good biocompatibility (Kaivosoja et al., 2013). Therefore, the biocompatibility of ta-C+CNT was compared to that of ta-C. Fig. 4 shows that the mNSCs mainly grew in clusters and no major differences between cell morphology on ta-C and ta-C+CNT could be observed. The morphology is typical for mNSCs, and some cells grown on bare ta-C showed particularly well spread morphology (Figure 4 A).

Although mNSCs generally require poly-l-lysine (PLL) coating for adhesion, we have observed that mNSC adhesion on ta-C is particularly good and MTT assay measured from mNSCs is similar on ta-C with and without PLL coating (not shown). In comparison, significant increase in MTT is measured, for example, on pyrolytic carbon with PLL coating compared to pyrolytic carbon without any coatings (Peltola, Heikkinen et al., 2017).

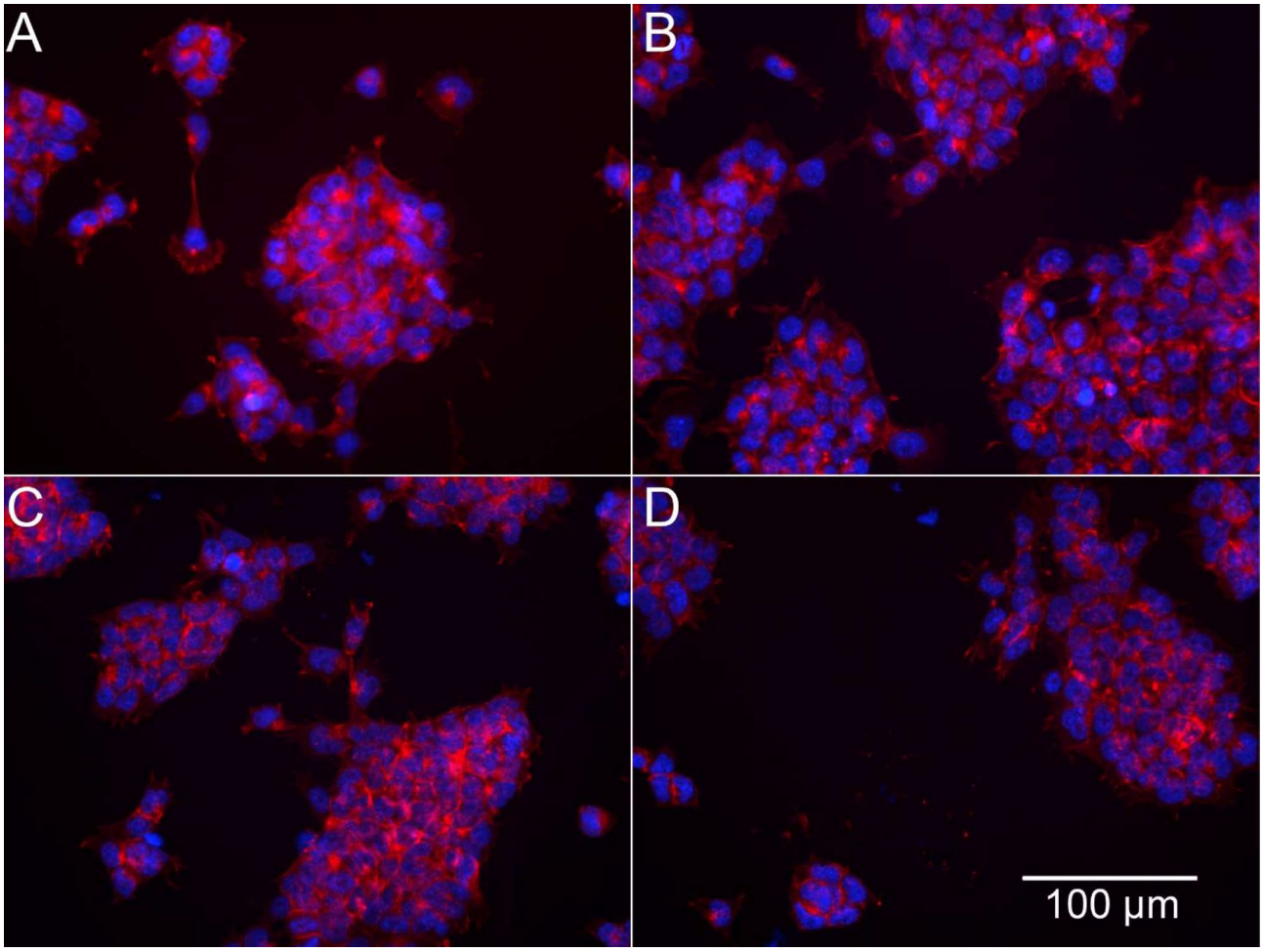

***Figure 4**. Morphology of the mouse neural stem cells grown on A) ta-C 15 nm, B) ta-C 50 nm, C) 15 nm ta-C+CNT and D) 50 nm ta-C+CNT. Actin cytoskeletons are visualized as red and cell nuclei as blue.*

Commonly used cytotoxicity evaluation methods, such as MTT, are not appropriate for the quantitative toxicity assessment of MWCNTs as MTT-formazan crystals formed in the MTT reaction are lumped with MWCNTs causing unreliable results (Casey et al., 2007, Wörle-Knirsch et al., 2006). Here, we evaluated cell viability by counting the cells from fluorescence microscopy images. The number of cells was approximately the same with no statistically significant differences between the materials (Fig. S3). Based on cell count and morphology visualization, bare ta-C and ta-C+CNT exhibited good biocompatibility for mNSCs.

4. Conclusions

Unmodified and MWCNT-modified ta-C films of 15 and 50 nm were evaluated as potential in vivo sensor materials for the detection of dopamine. The electroanalytical performance was investigated with CV, since it offers the required temporal resolution with sufficient sensitivity and selectivity to be used in in vivo conditions. The detection limits ranged from 40 to 85 nM, which are well within the physiologically meaningful range for in vivo measurement of dopamine. The 50 nm ta-C and 50 nm ta-C+CNT electrodes had better LOD values than the corresponding electrodes with 15 nm ta-C, which was due to the lower capacitive background current and smaller standard deviation of blank CVs in both cases. Although the modification of the ta-C films with MWCNTs did not improve the limits of detection, it did confer the necessary selectivity to detect simultaneously dopamine and its main interferents, ascorbic acid and uric acid, at physiologically relevant concentrations. Unmodified ta-C electrodes could not resolve between the

oxidation peaks of the three analytes. Cell culture of mNSCs on ta-C and ta-C+CNT indicated that both materials have good biocompatibility. Based on their electroanalytical performance and their good biocompatibility, ta-C and ta-C+CNT are attractive materials for electroanalytical applications with potential use as in vivo sensors. Future work is needed to address the effect of the observed structural differences between the 15 and 50 nm ta-C+CNT electrodes on their electrochemical properties and the underlying causes of the large cathodic shift of the oxidation potential of AA.

Acknowledgements

The authors acknowledge D.Sc. Hua Jiang for taking the TEM micrographs and M.Sc. Elli Leppänen for helping with electrode fabrication. This work was supported by the Academy of Finland (E.P. grant #274670, T.P. and T.L. grant #285526). The authors also acknowledge the provision of facilities at the Nanomicroscopy Center and at Micronova Nanofabrication Center by Aalto University and Center of Microscopy and Nanotechnology by University of Oulu.

References

Antunes, E., Lobo, A., Corat, E., Trava-Airoldi, V., Martin, A., Veríssimo, C., 2006. Carbon. 44, 2202-2211.

Beamson, G, Briggs, D., 1992. High resolution XPS of organic polymers. Wiley, Chichester.

Bokobza, L., Bruneel, J., Couzi, M., 2013. Chem. Phys. Lett. 590, 153-159.

Casey, A., Herzog, E., Davoren, M., Lyng, F., Byrne, H., Chambers, G., 2007. Carbon. 45, 1425-1432.

Dumitrescu, I., Unwin, P.R., Macpherson, J.V., 2009. Chem. Commun., 6886-6901.

Dursun, Z., Gelmez, B., 2010. Electroanal. 22, 1106-1114.

Etula, J., Wester, N., Sainio, S., Laurila, T., Koskinen, J., 2018. unpublished work.

Ford, C.P., Gantz, S.C., Phillips, P.E., Williams, J.T., 2010. J. Neurosci. 30, 6975-6983.

Goto, T., Yasukawa, T., Kanda, K., Matsui, S., Mizutani, F., 2011. Anal. Sci. 27, 91-94.

Gusmão, R., Sofer, Z., Nováček, M., Pumera, M., 2016. ChemElectroChem. 3, 1713-1719.

Holt, K.B., Ziegler, C., Caruana, D.J., Zang, J., Millán-Barrios, E.J., Hu, J., Foord, J.S., 2008. Phys. Chem. Chem. Phys. 10, 303-310.

Huang, J., Liu, Y., Hou, H., You, T., 2008. Biosens. Bioelectron. 24, 632-637.

Jarošová, R., Rutherford, J., Swain, G.M., 2016. Analyst. 141, 6031-6041.

Johansson, L., Campbell, J.M., 2004. Surf. Interface Anal. 36, 1018-1022.

Justice Jr, J., 1993. J. Neurosci. Methods. 48, 263-276.

Kaivosoja, E., Suvanto, P., Barreto, G., Aura, S., Soininen, A., Franssila, S., Konttinen, Y.T., 2013. J. Biomed. Mater. Res. 101A, 842-852.

Khun, N., Liu, E., 2009. Electrochim. Acta. 54, 2890-2898.

Kim, J., Bordeanu, A., Pyun, J., 2009. Biosens. Bioelectron. 24, 1394-1398.

Kohen, R., Nyska, A., 2002. Toxicol. Pathol. 30, 620-650.

Laurila, T., Sainio, S., Jiang, H., Palomäki, T., Pitkänen, O., Kordas, K., Koskinen, J., 2015. Diam. Relat. Mater. 56, 54-59.

Laurila, T., Sainio, S., Caro, M.A., 2017. Prog. Mater. Sci. 88, 499-594.

Laurila, T., Protopopova, V., Rhode, S., Sainio, S., Palomäki, T., Moram, M., Feliu, J.M., Koskinen, J., 2014. Diam. Relat. Mater. 49, 62-71.

Levon, J., Myllymaa, K., Kouri, V., Rautemaa, R., Kinnari, T., Myllymaa, S., Konttinen, Y.T., Lappalainen, R., 2010. J. Biomed. Mater. Res. A. 92, 1606-1613.

Liu, L.X., Liu, E., 2005. Surf. Coat. Technol. 198, 189-193.

Ma, X., Jia, L., Zhang, L., Zhu, L., 2014. Chem. Eur. J. 20, 4072-4076.

Maalouf, R., Soldatkin, A., Vittori, O., Sigaud, M., Saikali, Y., Chebib, H., Loir, A., Garrelie, F., Donnet, C., Jaffrezic-Renault, N., 2006. Mater. Sci. Eng. C. 26, 564-567.

Mark Wightman, R., 1988. Anal. Chem. 60, 769A-779A.

McCreery, R.L., 2008. Chem. Rev. 108, 2646-2687.

Medeiros, R.A., Matos, R., Benchikh, A., Saidani, B., Debiemme-Chouvy, C., Deslouis, C., Rocha-Filho, R.C., Fatibello-Filho, O., 2013. Anal. Chim. Acta. 797, 30-39.

Oh, J., Yoon, Y.W., Heo, J., Yu, J., Kim, H., Kim, T.H., 2016. Talanta. 147, 453-459.

Palomäki, T., Wester, N., Caro, M.A., Sainio, S., Protopopova, V., Koskinen, J., Laurila, T., 2017. Electrochim. Acta. 225, 1-10.

Palomäki, T., Chumillas, S., Sainio, S., Protopopova, V., Kauppila, M., Koskinen, J., Climent, V., Feliu, J.M., Laurila, T., 2015. Diam. Relat. Mater. 59, 30-39.

Peltola, E., Heikkinen, J.J., Sovanto, K., Sainio, S., Aarva, A., Franssila, S., Jokinen, V., Laurila, T., 2017. J. Mater. Chem. B. 5, 9033-9044.

Peltola, E., Wester, N., Holt, K.B., Johansson, L., Koskinen, J., Myllymäki, V., Laurila, T., 2017. Biosens. Bioelectron. 88, 273-282.

Pimenta, M., Dresselhaus, G., Dresselhaus, M.S., Cancado, L., Jorio, A., Saito, R., 2007. Phys. Chem. Chem. Phys. 9, 1276-1290.

Pumera, M., 2012. Chem. Rec. 12, 201-213.

Qiu, J., Haubold, L., Swain, G.M., 2015. Anal. Methods. 7, 4481-4485.

Reiber, H., Ruff, M., Uhr, M., 1993. Clin. Chim. Acta. 217, 163-173.

Rice, M.E., 2000. Trends Neurosci. 23, 209-216.

Robertson, J., 2002. Mater. Sci. Eng. R. 37, 129-281.

Robinson, D.L., 2001. Neuroreport. 12, 2549-2552.

Robinson, D.L., Heien, M.L., Wightman, R.M., 2002. J. Neurosci. 22, 10477-10486.

Robinson, D.L., Hermans, A., Seipel, A.T., Wightman, R.M., 2008. Chem. Rev. 108, 2554-2584.

Ross, S.B., 1991. J. Neurochem. 56, 22-29.

Sainio, S., Palomäki, T., Rhode, S., Kauppila, M., Pitkänen, O., Selkälä, T., Toth, G., Moram, M., Kordas, K., Koskinen, J., 2015. Sens. Actuators B: Chem. 211, 177-186.

Scott, C.L., Pumera, M., 2011. Electrochem. Commun. 13, 426-428.

Sopchak, D., Miller, B., Kalish, R., Avyigal, Y., Shi, X., 2002. Electroanal. 14, 473-478.

Sun, C., Lee, H., Yang, J., Wu, C., 2011. Biosens. Bioelectron. 26, 3450-3455.

Tan, C., Dutta, G., Yin, H., Siddiqui, S., Arumugam, P.U., 2018. Sens. Actuators B: Chem. 258, 193-203.

Tritsch, N., Sabatini, B., 2012. Neuron. 76, 33-50.

Tsierkezos, N.G., Othman, S.H., Ritter, U., Hafermann, L., Knauer, A., Köhler, J.M., Downing, C., McCarthy, E.K., 2016. Sens. Actuators B: Chem. 231, 218-229.

Wang, Z., Shoji, M., Ogata, H., 2011. Analyst. 136, 4903-4905.

Wester, N., Sainio, S., Palomäki, T., Nordlund, D., Singh, V., Johansson, L., 2017. J. Phys. Chem. C.

Wörle-Knirsch, J., Pulskamp, K., Krug, H., 2006. Nano Lett. 6, 1261-1268.

Yang, G., Liu, E., Khun, N.W., Jiang, S.P., 2009. J. Electroanal. Chem. 627, 51-57.

Yang, X., Haubold, L., DeVivo, G., Swain, G.M., 2012. Anal. Chem. 84, 6240-6248.

Yoo, K., Miller, B., Kalish, R., Shi, X., 1999. Electrochem. Solid-State Lett. 2, 233-235.

Zeng, A., Neto, V.F., Gracio, J.J., Fan, Q.H., 2014. Diam. Relat. Mater. 43, 12-22.

Zhang, W., Chen, J., Li, Y., Yang, W., Zhang, Y., Zhang, Y., 2017. RSC Adv. 7, 5628-5635.